– Supporting Information –

Static and Dynamic Magnetic Properties of the Ferromagnetic Coordination Polymer $[Co(NCS)_2(py)_2]_n$

Michał Rams, Michael Böhme, Vladislav Kataev, Yulia Krupskaya, Bernd Büchner, Winfried Plass, Tristan Neumann, Zbigniew Tomkowicz and Christian Näther

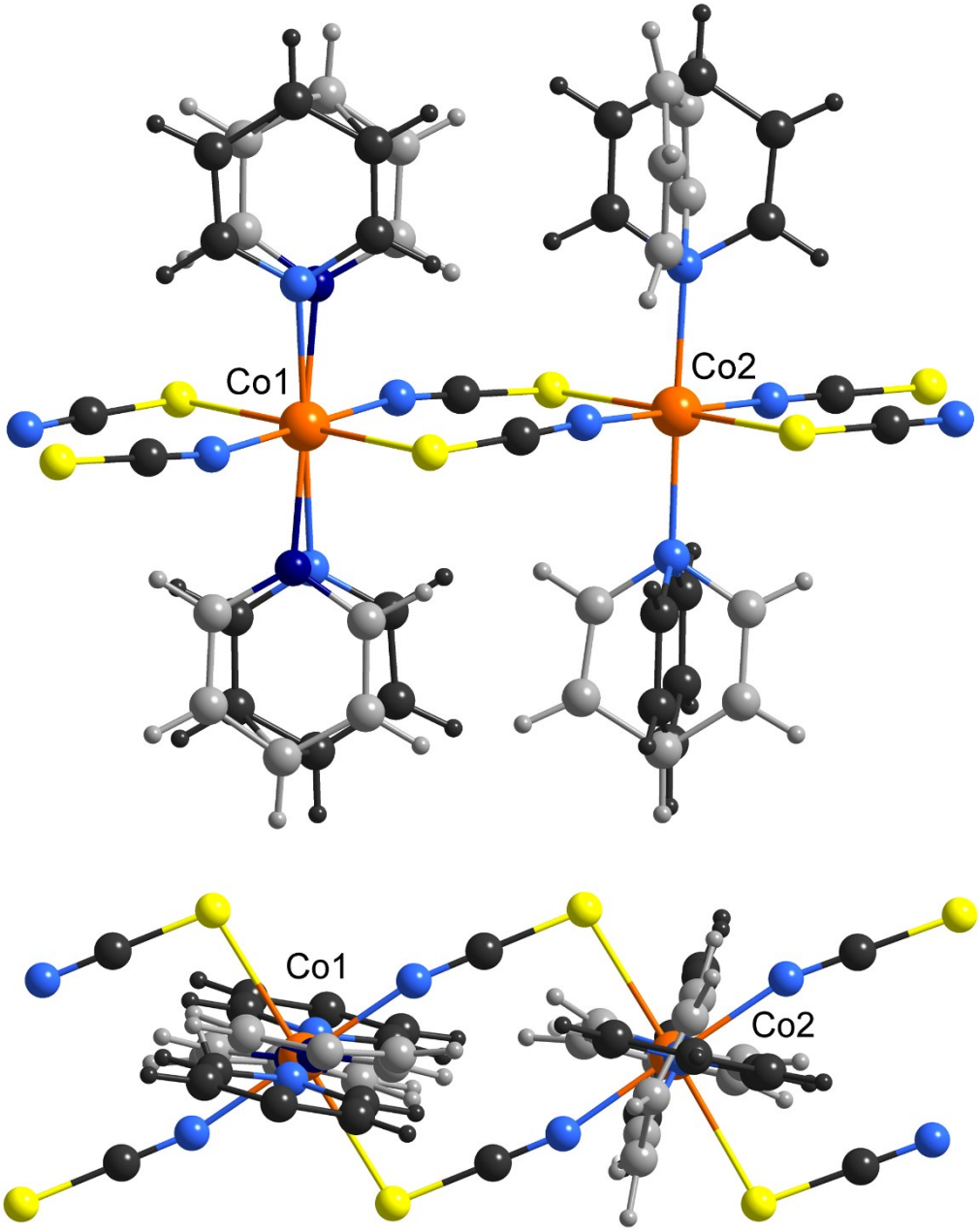

Figure S1. Side and top view of the $Co(NCS)_2$ chain showing the disorder of the pyridine ligands with the major orientation (85%) shown in dark grey and the minor orientation in light grey (15%). Please note that for the minor orientation the pyridine rings are still parallel for Co1 and rotated by about 90° for Co2.

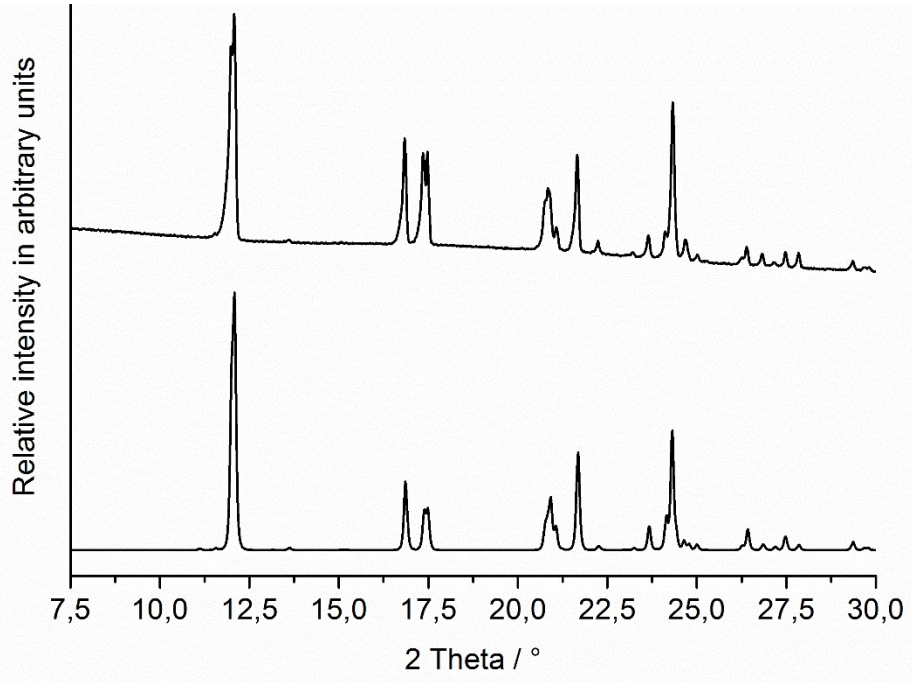

Figure S2. Experimental (top) and calculated (bottom) XRPD pattern of $[Co(NCS)_2(py)_2]_n$.

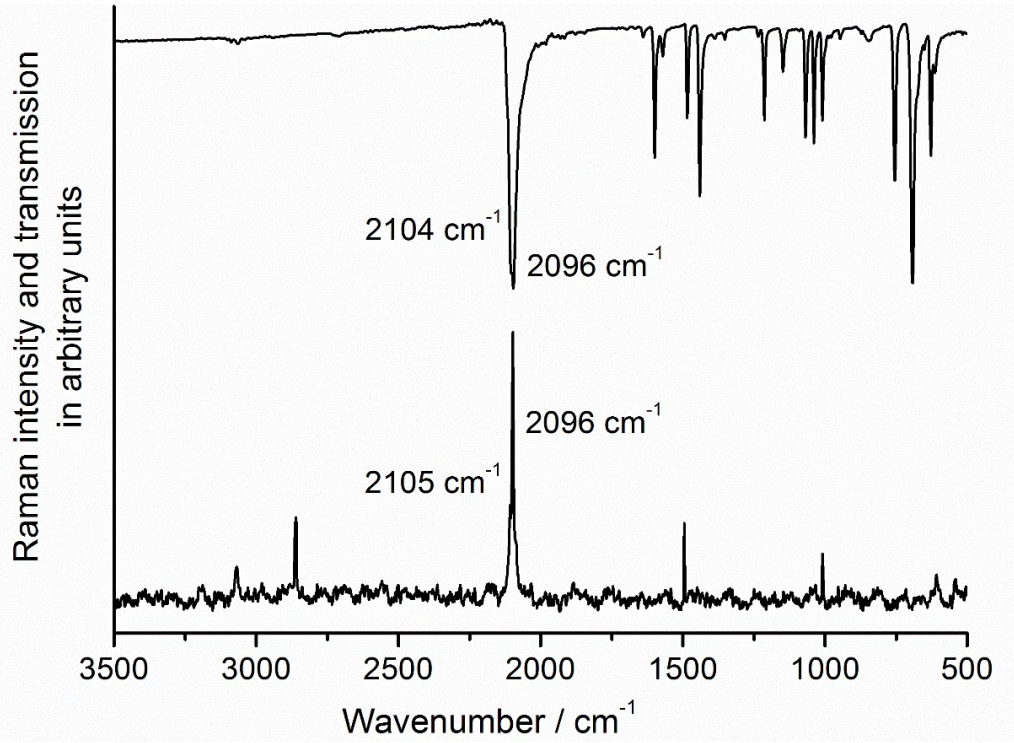

Figure S3. IR (top) and Raman (bottom) spectra of $[Co(NCS)_2(py)_2]_n$.

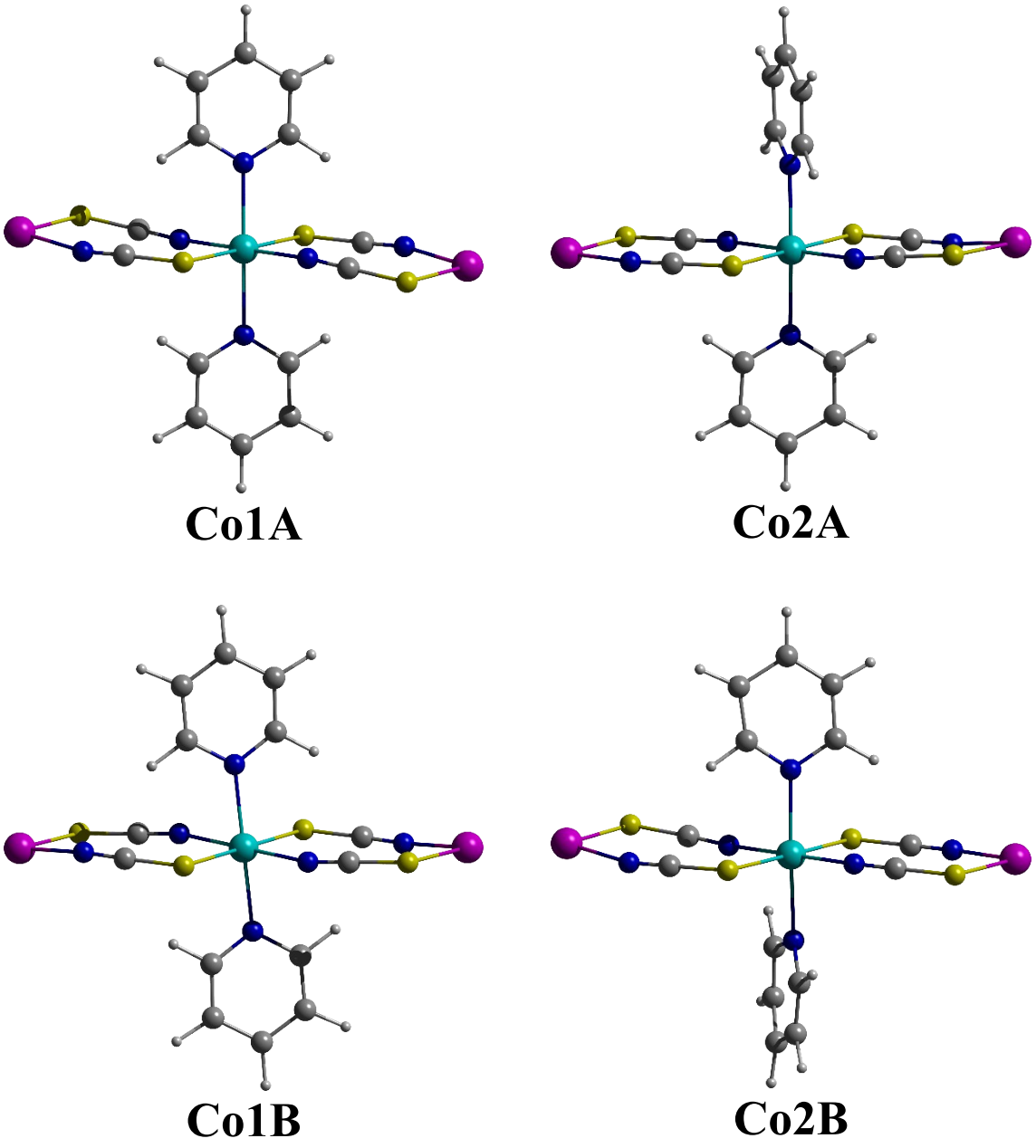

Figure S4. Models for the *ab initio* calculations for the two crystallographically independent cobalt(II) centers (Co1 and Co2) representing the observed disorder of the pyridine co-ligands in the structure of the polymer chain. (Top) Major component with an occupation factor of 0.85 denoted as **Co1A** and **Co2A**. (Bottom) Minor component with an occupation factor of 0.15 denoted as **Co1B** and **Co2B**. The pink spheres designate sodium(I) cations to compensate the negative charges of the mononuclear fragments.

Table S1. Relative energies for all quartet and the 12 lowest doublet states derived from *ab initio* CASSCF and CASPT2 calculations (in cm^{-1})

2*S*+1	Term		**Co1A**		**Co2A**		**Co1B**		**Co2B**	
			CASSCF	CASPT2	CASSCF	CASPT2	CASSCF	CASPT2	CASSCF	CASPT2
4	^{4}F	$^4T_{1g}$	0	0	0	0	0	0	0	0
			392	861	136	45	346	89	117	225
			490	1234	334	1212	1193	1314	349	973
		$^4T_{2g}$	5170	6389	5197	6428	5600	6480	5192	6403
			7360	8589	7366	8606	8375	8427	7177	8329
			8280	9269	8270	9261	8722	9057	8213	9224
		$^4A_{2g}$	14947	17048	15087	17204	15970	17624	14882	16907
	^{4}P	$^4T_{1g}$	21342	21456	21489	21595	21573	18067	21298	20223
			22010	18259	21912	18057	22782	21389	21982	19100
			25629	25561	25392	25201	26850	26695	25253	25009
2	^{2}G + ^{2}P		12013	9431	11821	9151	11409	8131	11959	9373
			15850	13716	15438	13218	15769	13092	15467	13235
			17666	15967	17627	15880	17773	14604	17640	15887
			18473	16518	18406	16395	17936	15361	18534	16585
			19063	17002	19000	16871	19196	16641	19003	16826
			20096	18058	19833	17673	20140	18251	19836	17783
			20275	18979	20099	18759	20670	18388	20097	18575
			21095	19051	20996	18849	21356	18607	20953	18727
			24111	21908	24129	19559	23675	20555	24056	21433
			24433	23479	24370	19680	24983	23465	24358	23404
			24495	21737	24417	23418	25020	22173	24465	21817
			24874	22921	24805	22676	25204	22759	24761	22501
	…		…	…	…	…	…	…	…	…

Table S2. Relative energies for the Kramers doublets of the $^4T_{1g}$ multiplet derived from *ab initio* CASSCF/CASPT2/RASSI-SO calculations (in cm^{-1})

Kramers doublet	**Co1A**	**Co2A**	**Co1B**	**Co2B**
1	0	0	0	0
2	192	259	230	238
3	757	529	688	554
4	972	816	969	825
5	1923	1733	1848	1626
6	1977	1781	1922	1685

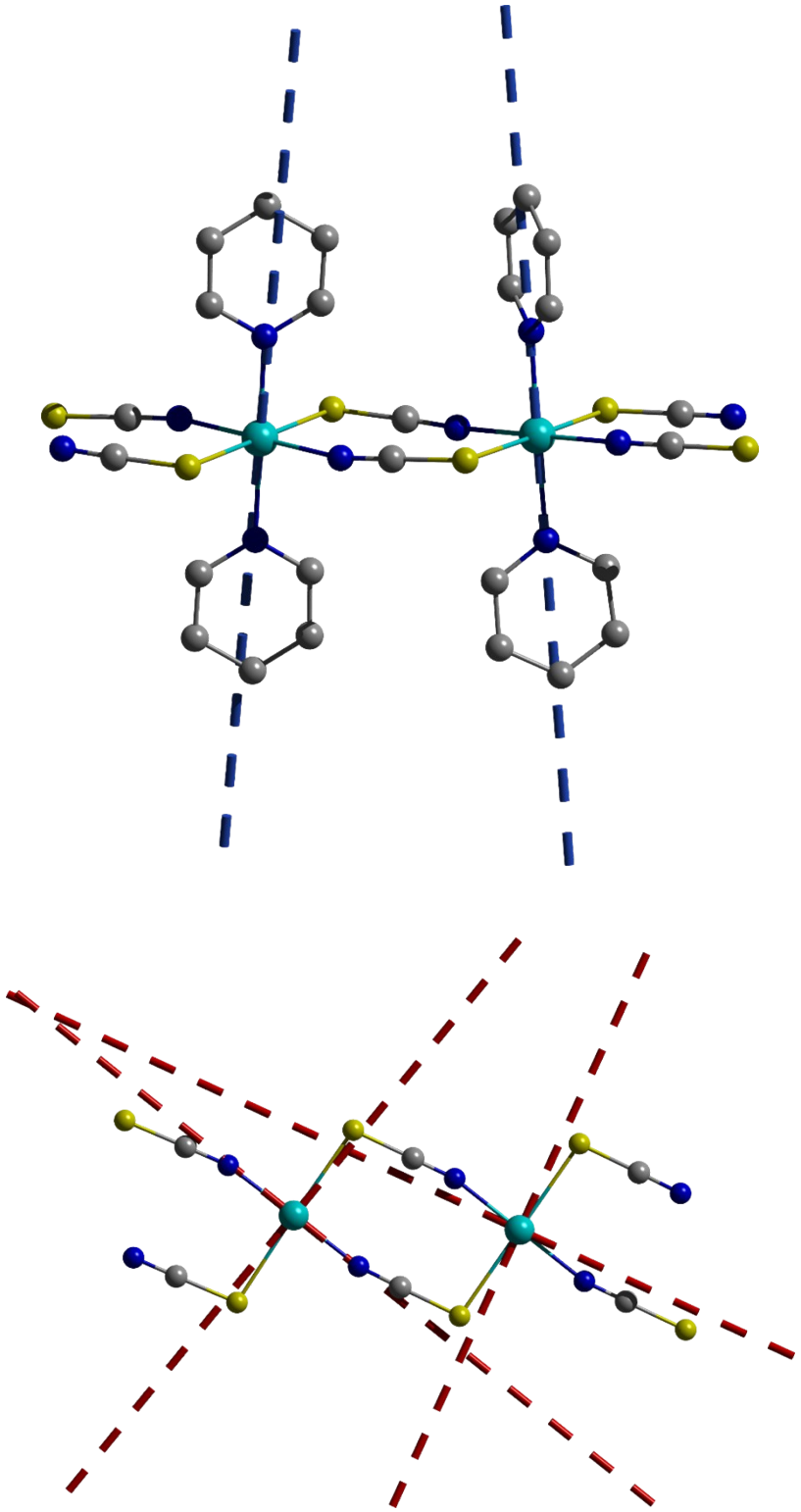

Figure S5. Representation of the magnetic axes derived from *ab initio* calculations (S_{eff} = 1/2) for **Co1A** and **Co2A** projected onto a dinculear cobalt(II) chain fragment (blue dashed lines: g_z; red dashed lines: g_x and g_y). (Top) Complete fragment (hydrogen atoms omitted for clarity). (Bottom) View along the Co–N_{py} axes (pyridine ligands removed for clarity). The angle between both g_z axes is 13.8°.

Table S3. Main components of the *g* tensor (S_{eff} = 1/2) and their relative energies for the first two Kramers doublets of **Co1B** and **Co2B** obtained from *ab initio* calculations (CASSCF/CASPT2/RASSI-SO)

		Co1B	**Co2B**
KD1	E_{KD1} / cm^{-1}	0	0
	g_x	1.056	1.600
	g_y	1.402	2.321
	g_z	8.876	8.163
KD2	E_{KD2} / cm^{-1}	230	238
	g_x	4.083	3.933
	g_y	3.698	2.969
	g_z	2.595	1.947

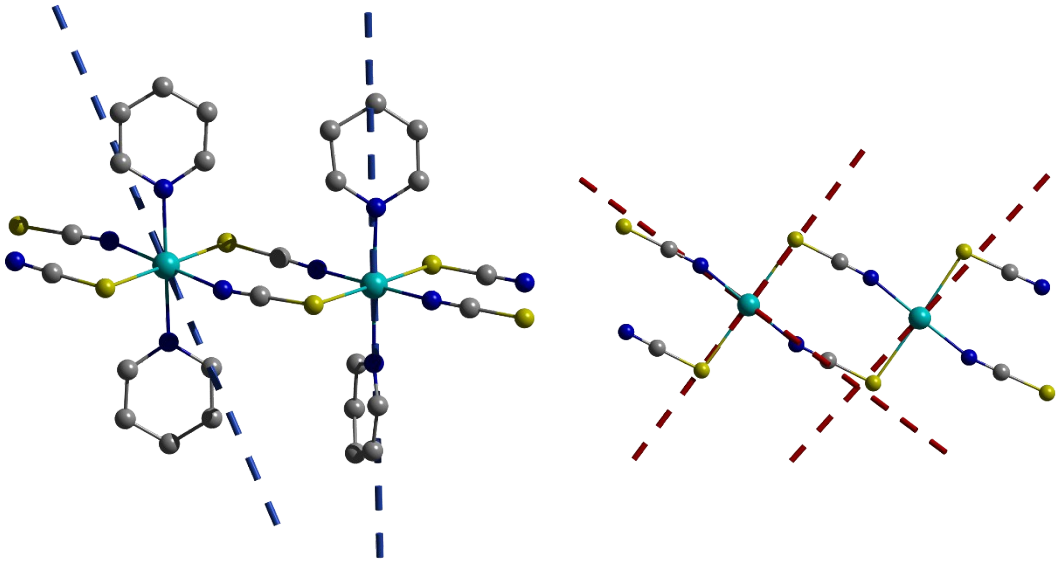

Figure S6. Representation of the magnetic axes derived from *ab initio* calculations (S_{eff} = 1/2) for **Co1B** and **Co2B** projected onto a dinuclear Co(II) chain fragment (blue dashed lines: g_z; red dashed lines: g_x and g_y). (Left) Complete fragment (hydrogen atoms omitted for clarity). (Right) View along the Co–N_{py} axes (pyridine ligands removed for clarity). The angle between both g_z axes is 27.5°.

Table S4. Main components of the *g* tensor (S_{eff} = 1/2) and their relative energies for **Co1A** and **Co2A** with terminal zinc(II) cations instead of sodium(I) cations (see pink spheres in Figure S1) obtained from *ab initio* calculations (CASSCF/CASPT2/RASSI-SO), note the change in the model is to investigate the influence of the cation charge on the calculated *g* components

		Co1A	**Co2A**
KD1	E_{KD1} / cm^{-1}	0	0
	g_x	2.097	1.977
	g_y	4.231	2.466
	g_z	6.367	7.866
KD2	E_{KD2} / cm^{-1}	182	238
	g_x	0.863	1.661
	g_y	1.093	2.665
	g_z	5.438	4.166

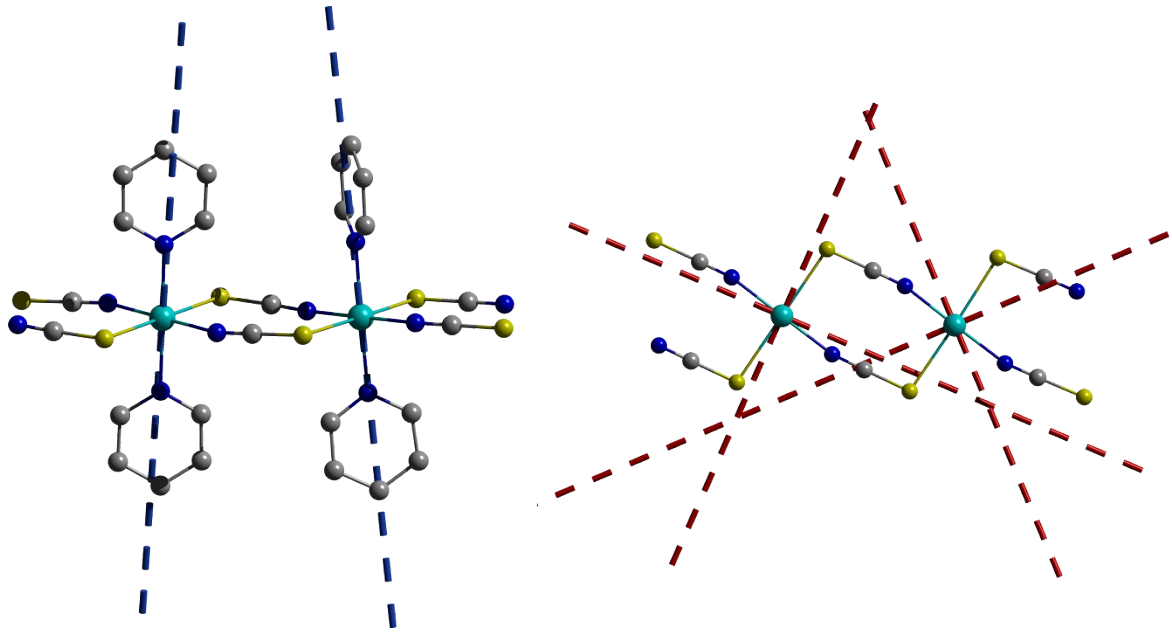

Figure S7. Representation of the magnetic axes derived from *ab initio* calculations (S_{eff} = 1/2) for **Co1A** and **Co2A** with terminal zinc(II) cations instead of sodium(I) cations (see pink spheres in Figure S4) projected onto a dinculear cobalt(II) chain fragment (blue dashed lines: g_z; red dashed lines: g_x and g_y). (Left) Complete fragment (hydrogen atoms omitted for clarity). (Right) View along the Co–N_{py} axes (pyridine ligands removed for clarity). The angle between both g_z axes is 14.7°.

Table S5. Calculated ZFS and *g* tensor parameters for the two lowest Kramers doublets of the $^4T_{1g}$ term ($S_{eff} = 3/2$) for the cobalt(II) centers of the minor components **Co1B** and **Co2B** in the disordered structure obtained from *ab initio* calculations (CASSCF/CASPT2/RASSI-SO)

	Co1B	**Co2B**
D / cm^{-1}	−108.6	103.9
E / cm^{-1}	−21.7	33.3
E / D	0.20	0.32
g_x	1.817	1.703
g_y	2.201	2.294
g_z	3.190	3.126

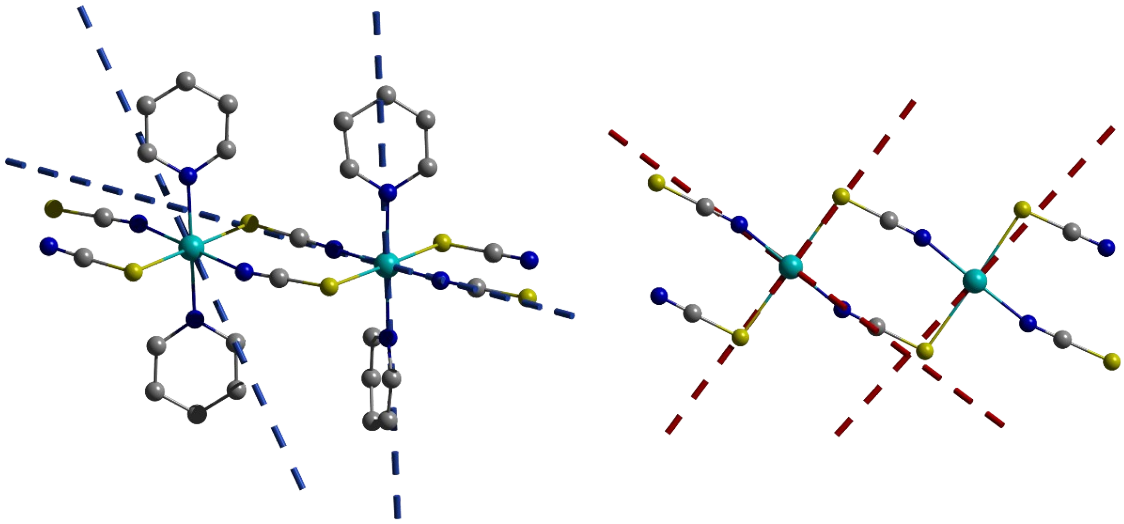

Figure S8. Representation of the magnetic axes derived from *ab initio* calculations (S_{eff} = 3/2) for **Co1B** and **Co2B** projected onto a dinculear cobalt(II) chain fragment (blue dashed lines: g_z; red dashed lines: g_x and g_y). (Left) Complete fragment (hydrogen atoms omitted for clarity). (Right) View along the Co–N_{py} axes (pyridine ligands removed for clarity). **Co2B** shows an easy-plane anisotropy (angle between **Co1B** easy-axis and **Co2B** easy-plane: 85.5°) in contrast to **Co1B**, **Co1A**, and **Co2A**, which is most likely due to the observed disorder.

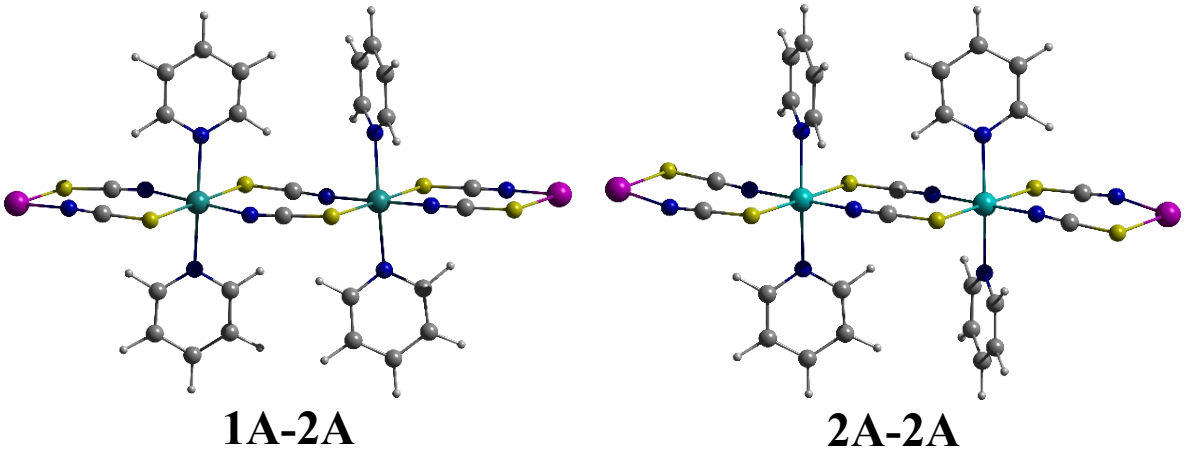

Figure S9. BS-DFT computational models for the different magnetic couplings $J_{1A\text{-}2A}$ and $J_{2A\text{-}2A}$. The pink spheres designate either zinc(II) or sodium(I) cations to compensate the negative charge to obtain a better charge distribution in the dinuclear cobalt(II) model fragments for the $[Co(NCS)_2(py)_2]_n$ coordination chain.

Table S6. BS-DFT results for the two Heisenberg coupling constants ($J_{1A\text{-}2A}$ and $J_{2A\text{-}2A}$) depending on the choice of the terminal cations (zinc(II) and sodium(I) cation, see pink spheres in Figure S9)

Computational model		J / K	$2S+1$	E_{rel} / Hartree	$\langle S^2 \rangle$
$[Co_2Zn_2(NCS)_6(py)_4]^{2+}$	$J_{1A\text{-}2A}$	6.2	7	−10260.57410	12.066
			1	−10260.57401	3.062
	$J_{2A\text{-}2A}$	15.1	7	−10260.56001	12.059
			1	−10260.55980	3.059
$[Co_2Na_2(NCS)_6(py)_4]$	$J_{1A\text{-}2A}$	2.3	7	−7027.34575	12.019
			1	−7027.34572	3.017
	$J_{2A\text{-}2A}$	−9.6	7	−7027.34802	12.020
			1	−7027.34816	3.018

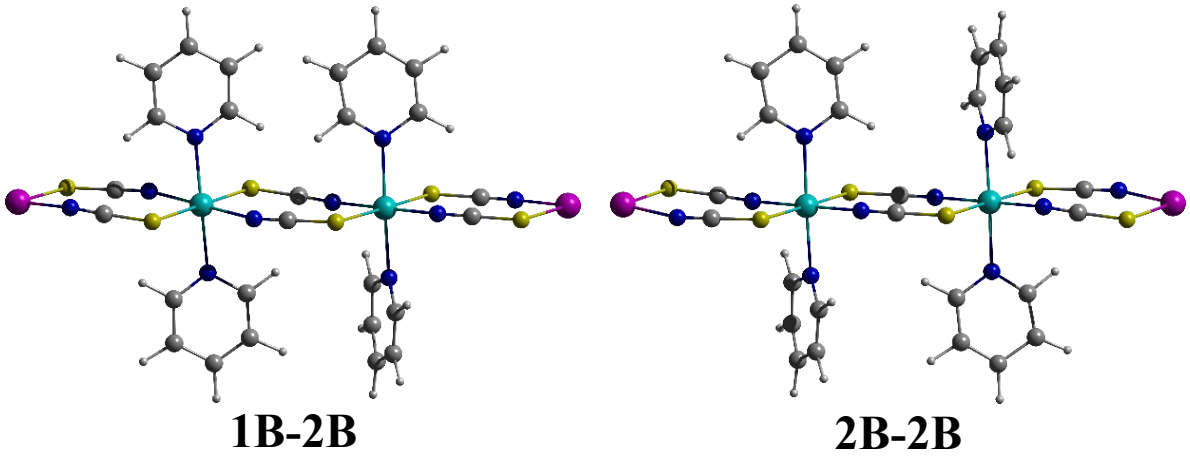

Figure S10. BS-DFT computational models for the different magnetic couplings $J_{1B\text{-}2B}$ and $J_{2B\text{-}2B}$. The pink spheres designate either zinc(II) or sodium(I) cations to compensate the negative charge to obtain a better charge distribution in the dinuclear cobalt(II) model fragments for the $[Co(NCS)_2(py)_2]_n$ coordination chain.

Table S7. BS-DFT results for the two Heisenberg coupling constants ($J_{1B\text{-}2B}$ and $J_{2B\text{-}2B}$) depending on the choice of the terminal cations (zinc(II) and sodium(I) cation, see pink spheres in Figure S10)

Computational model		J / K	$2S+1$	E_{rel} / Hartree	$\langle S^2 \rangle$
$[Co_2Zn_2(NCS)_6(py)_4]^{2+}$	$J_{1B\text{-}2B}$	1.5	7	−10260.51228	12.047
			1	−10260.51226	3.046
	$J_{2B\text{-}2B}$	0.9	7	−10260.50516	12.076
			1	−10260.50514	3.070
$[Co_2Na_2(NCS)_6(py)_4]$	$J_{1B\text{-}2B}$	−7.6	7	−7027.28455	12.019
			1	−7027.28466	3.017
	$J_{2B\text{-}2B}$	−50.2	7	−7027.27857	12.019
			1	−7027.27929	3.018

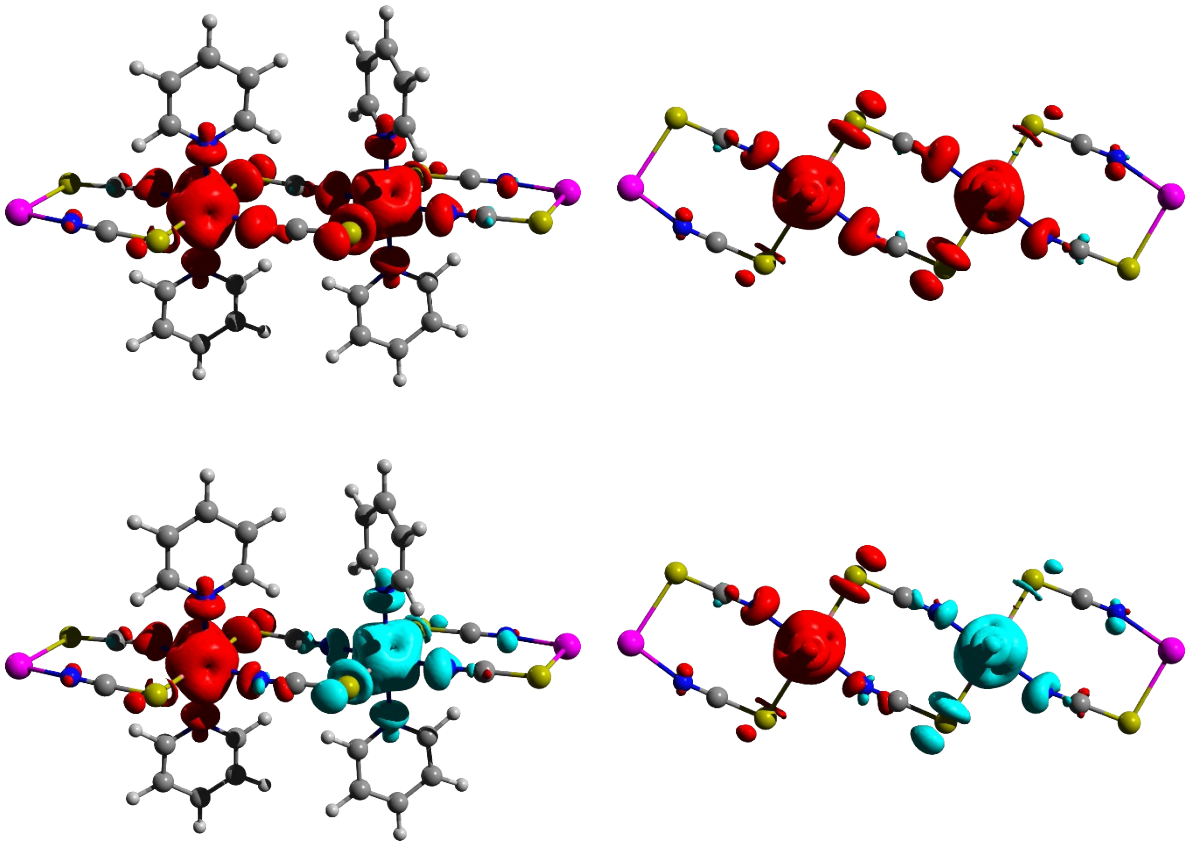

Figure S11. BS-DFT obtained spin densities for **1A-2A** (first row: high-spin state, second row: broken-symmetry state). Red (cyan) isosurfaces represent net α (β) spin densities (iso-value 0.002). The two pictures on the right-hand side show a view from the top without the pyridine ligands.

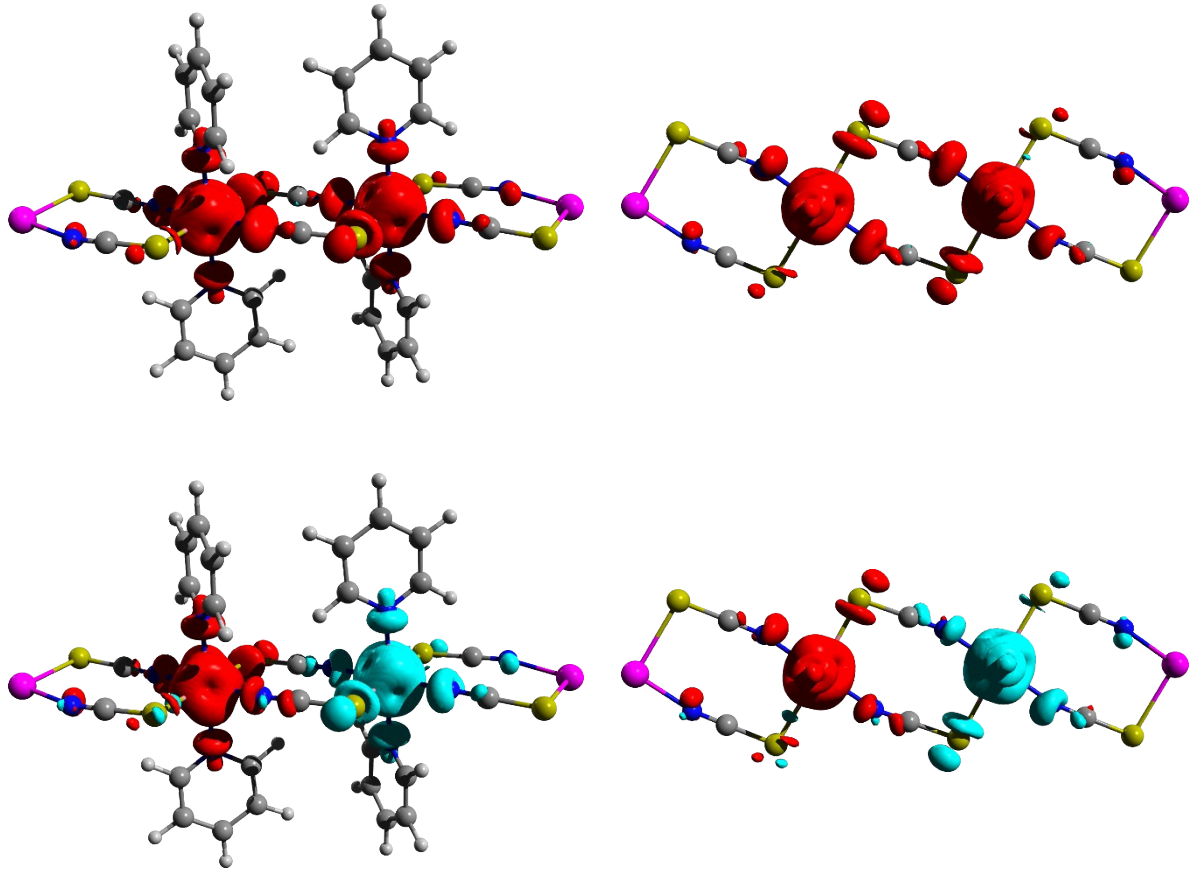

Figure S12. BS-DFT obtained spin densities for **2A-2A** (first row: high-spin state, second row: broken-symmetry state). Red (cyan) isosurfaces represent net α (β) spin densities (iso-value 0.002). The two pictures on the right-hand side show a view from the top without the pyridine ligands.